Lévy-distributed fluctuations in the living cell cortex

Shankar Sivarajan,[1] Yu Shi,[1] Katherine M. Xiang,[1] Clary Rodríguez-Cruz,[2] Christopher L. Porter,[2] Geran M. Kostecki,[3] Leslie Tung,[3] John C. Crocker,[2,*] and Daniel H. Reich[1,†]

[1]*Department of Physics and Astronomy, Johns Hopkins University, Baltimore, Maryland 21218, USA*

[2]*Department of Chemical and Biomolecular Engineering, University of Pennsylvania, Philadelphia, Pennsylvania 19104, USA*

[3]*Department of Biomedical Engineering, Johns Hopkins University, Baltimore, Maryland 21205, USA*

(Received 21 August 2023; accepted 15 November 2024; published 12 December 2024)

The actomyosin cortex is an active material that provides animal cells with a strong but flexible exterior whose mechanics, including non-Gaussian fluctuations and occasional large displacements or cytoquakes, have defied explanation. We study the active fluctuations of the cortex using nanoscale tracking of arrays of flexible microposts adhered to multiple cultured cell types. When the confounding effects of static heterogeneity and tracking error are removed, the fluctuations are found to be heavy tailed and well described by a truncated Lévy α-stable distribution over a wide range of timescales, in multiple cell types. The largest random displacements closely resemble the earlier-reported cytoquakes, but notably, we find these cytoquakes are not due to earthquakelike cooperative rearrangement of many cytoskeletal elements. Rather, they are indistinguishable from chance large excursions of a superdiffusive random process driven by heavy-tailed noise. The noncooperative microscopic events driving these fluctuations need not be larger than the expected elastic energy of single tensed cortical actin filaments, and the implied distribution of microscopic event energies will need to be accounted for by future models of the cytoskeleton.

DOI: 10.1103/PhysRevResearch.6.043265

I. INTRODUCTION

The actomyosin cortex is a thin sheet of active matter formed from actin filaments, crosslinking proteins and myosin contractile motors existing in a dynamic steady state. After decades of study both in cells [1–8] and in reconstituted gels [9,10], the mechanical properties of the actomyosin cortex are well known; it is a tensed, nearly elastic network that resists deformations via a dynamic shear modulus, which is a weak power law of frequency [1,2,4,7,8,11–13]. This sheet undergoes active fluctuations that are superdiffusive [14–16] and heavy tailed [8,17,18], but such measurements are often confounded by heterogeneity effects. These varied phenomena have not yet been reproduced by a physics-based model. Some models [19–21] predict power-law shear moduli but do not explain the non-Gaussian fluctuations. While Fredberg and colleagues [1,17] have long noted similarities between cytoskeletal networks and soft glassy materials (SGMs) such as foams and emulsions [22–25], with both displaying power-law rheology [22–28], superdiffusive dynamics [25–28], and non-Gaussian displacements [28], how foams and the cytoskeleton could obey the same physics remains an open question. More recently, the cortex has also been observed to undergo occasional large displacements in the plane [8,18,29], termed cytoquakes, which, due to their power-law displacement distribution and large energy scales, are hypothesized to be the result of earthquakelike cooperative rearrangement of many cytoskeletal elements. Such cooperative motion suggests the cortex may exist near a mechanical critical point, on the cusp of instability. Testing of different cytoquake models [30–32], however, is currently limited by the available data.

Here we report low-noise, high statistical power measurements of the lateral fluctuations and cytoquakes of the actomyosin cortex of multiple cell types. We used micropost array detectors (mPADs) consisting of dozens of flexible microposts anchored to cells' basal cortex. The data from each micropost was rescaled to correct for post-to-post heterogeneity, before being pooled together. While the largest post displacements resemble the previously reported cytoquakes, we find that their functional form is consistent with a stationary random process that is unlike that in earthquakes and other nonstationary (time-dependent) random processes. We find that the entire distribution of micropost displacements, from the nanoscale to the cytoquake scale, is well described by a Lévy α-stable distribution with an exponential truncation, resembling a recently described, stationary superdiffusive random process termed linear fractional stable motion (LFSM) [33,34]. Physically, such a process corresponds to a viscoelastic solid driven by non-Gaussian noise having a heavy-tailed amplitude distribution and naturally explains the previously reported power-law distribution of cortical displacements. This finding also provides a potential explanation for the similarity of the cortex and SGMs [26,27]—both may be

*Contact author: jcrocker@seas.upenn.edu
†Contact author: reich@jhu.edu

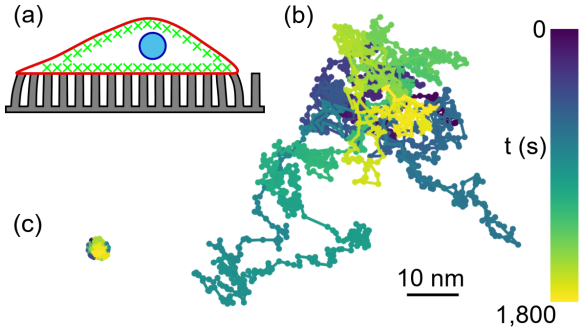

FIG. 1. (a) Schematic of a cell on a micropost array. Cellular traction forces deflect the posts, which are tracked optically. (b) The trajectory of a micropost ($k = 15.8\,\mathrm{nN/\mu m}$) coupled to the cortex of a 3T3 cell, over 1800 s, after time-averaging data recorded at 10 fps to 1 fps. (c) The trajectory of a micropost not coupled to the cell shows the measurement error.

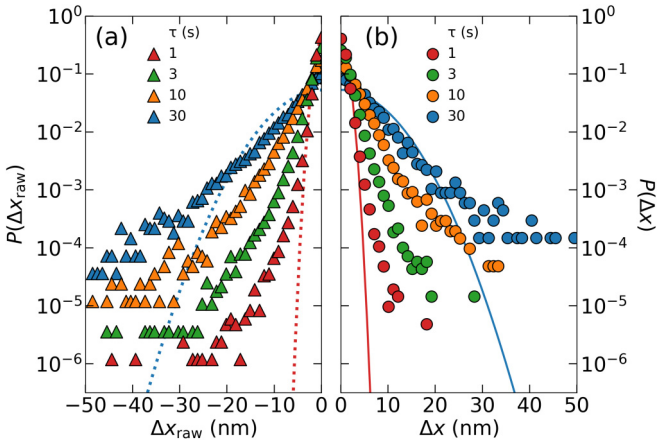

FIG. 2. The van Hove displacement distribution is heavy tailed even after post-to-post heterogeneity is removed. (a) Distribution of measured displacements $P(\Delta x_{\mathrm{raw}})$ for the x component of the post trajectories at fixed lag time τ for an ensemble of 336 posts from 10 3T3 cells. Post stiffness: $k = 15.8\,\mathrm{nN/\mu m}$ (medium stiffness). To facilitate comparison with panel (b), only the $\Delta x_{\mathrm{raw}} \leqslant 0$ half of the symmetric distribution is shown. (b) Van Hove distributions $P(\Delta x)$ following rescaling to remove static heterogeneity as described in the text. The data in (b) only include steps from posts in the uppermost quartile of the distribution of the trajectories' geometric means. Only the $\Delta x \geqslant 0$ half of the symmetric distribution is shown. The lines in (a) and (b) are best-fit Gaussians at $\tau = 1$ s and $\tau = 30$ s.

viscoelastic solids driven by heavy-tailed active noise [28]. Last, we estimate that the maximum energy of the microscopic processes driving the cortical fluctuations may be smaller than the energy in single tensed cortical actin filaments. Known microscopic energy release processes occurring during the rapid turnover of the cortex [35] appear sufficient to explain our fluctuation measurements and cytoquake observations without earthquakelike cooperativity. Our measurements are likely to be sensitive to cortical details such as the cortical actin filament energy distribution, related to filament tension and length, and may be useful to constrain future physical models of the actomyosin cortex.

II. EXPERIMENTAL METHODS

mPAD arrays are a well-established technique for quantifying cell mechanics and contractility [36–41]. A schematic of a cell on an mPAD array is shown in Fig. 1(a). Recently, we have demonstrated [8,29,42] that mPADs can be used to quantify cortical fluctuations with subnanometer precision. Building on this approach, for this study we used a poly(dimethylsiloxane) (PDMS) mPAD device platform [8,29,42] consisting of 1.8-μm-diameter microposts on hexagonal lattices with center-to-center spacing 4 μm. Micropost heights of 9.1, 6.4, and 5.7 μm were used, providing effective spring constants for small lateral deflections k of 5.5, 15.8, and 22.3 nN/μm [41], corresponding to substrate stiffnesses 4.3, 12, and 17 kPa [43]. [We refer to these as "low" (L), "medium" (M) and "high" (H) stiffness substrates.] The mPAD devices were functionalized to restrict cell adhesion to the micropost tops [36] (see Supplemental Material, SM, for methods [44]).

NIH 3T3 fibroblasts (ATCC), human embryonic kidney (HEK) cells (ATCC), human bone osteosarcoma epithelial cells (U2OS), and primary neonatal rat cardiac fibroblasts (CFs) were cultured and seeded on the mPADs as described previously [29]. Cardiac myofibroblasts (MFs) were produced from the CFs by treatment with TGF-β1 [29] prior to seeding. Bright-field videos of individual cells, of duration 30 min, were recorded at 10 frames per second (fps) or 100 fps (HEK and U2OS cells only) [8,42] (see methods discussed in SM [44]). A previous study [8] suggests that the cortex is stiffer than the micropost spring, allowing us to interpret post deflections as cortical displacements rather than forces. While the posts' spring-restoring force on the cortical displacements must limit the displacement amplitude, such effects have been shown to be small on the timescales studied here [8].

The trajectories of the posts $\mathbf{r}(t)$ were determined by a centroid tracking algorithm [8,42,45]. To improve resolution, the post centroids were time averaged to 1 fps, yielding a positional uncertainty of $\Delta x \approx 0.5$ nm. To isolate posts coupled to the cortex, we adapted and refined an approach reported previously [8,29,42], using the post trajectories' mean-squared displacements (MSDs), average traction force, displacement range, and non-Gaussian parameter to identify posts coupled to the cell, to distinguish cortically associated posts from stress-fiber-associated posts, and to screen out data perturbed by out-of-focus debris (see SM methods and Fig. S1 [44]).

III. MPADs REVEAL NANOMETER-SCALE MOTION OF THE CORTEX

Microposts attached to the cell cortex showed dynamic displacements on the 10-nm scale, driven by lateral cortical fluctuations, while background posts did not [Figs. 1(b) and 1(c)]. To characterize these random post/cortical displacements, we computed the van Hove self-correlation function, or the probability distribution of displacements $P(\Delta x_{\mathrm{raw}}(\tau))$ in a waiting (or lag) time τ. Figure 2(a) shows the displacement distribution for an ensemble of 336 posts from nine different 3T3 cells, for 1 s $\leqslant \tau \leqslant$ 30 s. At all lag times measured, the distributions were non-Gaussian with pronounced heavy tails at large $|\Delta x_{\mathrm{raw}}|$. Such measurements, which pool results

over many posts, are susceptible to confounding effects due to heterogeneity [11], such as variations in how different posts/tracers are coupled to the cytoskeleton, or differences between cells. Prior studies of cells' cortical displacements using single tracers [8,18] have yielded similar results to Fig. 2(a), suggesting that such fluctuations are not due solely to heterogeneity.

A pooled measurement of displacements can be corrected for heterogeneity by rescaling. In the case of *static heterogeneity*, each post i reports the time-dependent motion $x^i_{\rm raw}(t)$ of a segment of the cortex multiplied by a different, time-independent constant. This suggests that each post's motion can be rescaled by a single constant so as to have the same typical amplitude as the entire ensemble, e.g.,

$$\Delta x^i(t) = \Delta x^i_{\rm raw}(t)\left[\frac{\langle \mathrm{GM}(|\Delta x^i_{\rm raw}(\tau = 10\,\mathrm{s})|)\rangle_{\rm ens}}{\mathrm{GM}(|\Delta x^i_{\rm raw}(\tau = 10\,\mathrm{s})|)}\right], \qquad (1)$$

where GM(.) designates the geometric mean of a set of numbers, a robust measure of the typical value in heavy-tailed distributions, and $\langle . \rangle_{\rm ens}$ is an ensemble average over all posts. The choice to scale by the displacements at $\tau = 10$ s minimized the effects of measurement error while retaining good statistics. The distributions of post rescaling factors for our set of cell types and substrate stiffnesses are shown in Fig. S2 [44]. A control analysis showed that the rescaling factor was not significantly time dependent over our 30-min datasets; cell-to-cell variations were also small [44].

A potential concern with this rescaling procedure is the amplification of noise contributions from posts with small GMs. In addition to nonbiological sources of noise, such as camera noise, which can be quantified using the background posts, a second noise source can arise from fluctuations in the local optical density over a post due to internal cellular rearrangements [8]. From an assessment of the magnitude of such contributions (see SM and Fig. S3 [44]), we determined that these effects do not contribute significantly to the signal from posts whose GM is in the top quartile of the GM distribution, and so we used those posts for subsequent analysis.

Figure 2(b) shows the resulting pooled distribution of cortical displacements for 3T3 cells, corrected for static heterogeneity, for a range of lag times. This confirms that cortical fluctuations are intrinsically non-Gaussian, while our statistical power allows us to observe that such non-Gaussianity persists to long lag times. At the shortest lag time measured, $\tau = 1$ s, we find random displacements that are up to 40 times larger than the geometric mean, similar to reports for cytoquakes [18]. The results for our other experimental configurations and cell types, shown in Fig. S4 [44], show similar but somewhat less non-Gaussian behavior.

Visual examination of the trajectories corresponding to the largest displacements showed two qualitatively different kinds of events. The majority of the events were isotropically directed and showed roughly sigmoidal shapes with typical widths >1 s, while other events were very abrupt, with typical widths <1 s, and were strongly directed toward the posts' resting locations. Examples of such trajectories and their respective angular probability distributions are shown in Figs. S5(a)–S5(d) [44]. Given the tendency of the abrupt events to move toward the post's resting location, we hypothesize that they are due to transient loading of the cortex by stress fibers followed by detachment and/or de-adhesion events of the micropost from the cell [8]. Given that such processes are not fluctuations within the cortex itself, as might occur due to motor activity or remodeling, we screened the abrupt events out from our analyses below, except where noted.

IV. CYTOQUAKES DO NOT RESEMBLE EARTHQUAKELIKE EVENTS

The large displacement events we observe (filtering out the abrupt events) have both amplitudes and sigmoidlike time dependence resembling the cytoquakes we and others have observed previously [8,18,29]. We seek to apply statistical tests to the cytoquakes' time-dependent data to determine if they resemble cooperative processes like earthquakes and avalanches, perhaps superimposed on a background noise of other mechanical fluctuations. We begin by averaging short trajectory segments of many large cytoquake displacements together (selected from the heavy tails of the van Hove distribution). The results $\langle x_{i,s}(t)\rangle$ of scaling and averaging the 200 largest gradual displacements at $\tau = 10$ s for four representative cell types are shown in Figs. 3(a)–3(d). During this averaging, the trajectories $x_i(t)$ containing each large displacement were rescaled to pass through the points $(\tau/2, -1/2)$ and $(+\tau/2, +1/2)$ (see SM for calculation details [44]). Figure 3(e) shows a similar average of 40 abrupt displacements for comparison. The corresponding data for both gradual and abrupt events for these and our other cell types and substrate conditions are shown in Fig. S6 [44].

For a stationary (noncooperative) random process, the average of short trajectory segments rescaled as in Fig. 3 is predicted by the interpolation-extrapolation function (IEF) [46], which gives the conditional expectation value for a random walk constrained to pass through two points [here $(-\tau/2, -1/2)$ and $(+\tau/2, +1/2)$]. If the MSD of the stationary random process varies as MSD $\sim \tau^a$, then the IEF is given by

$$\mathrm{IEF}(t) = \frac{1}{2\tau^a}\left(\left|t + \frac{\tau}{2}\right|^a - \left|t - \frac{\tau}{2}\right|^a\right) \qquad (2)$$

(see SM for a derivation of this expression [44]).

The cytoquake events are well fit by the IEF form, Eq. (2), with the exponent as a free parameter, Figs. 3(a)–3(d), while the abrupt events, Fig. 3(e), are not. This agreement demonstrates that the cytoquakes' apparent time dependence is indistinguishable from what is obtained by merely sampling and averaging the largest excursions of a stationary superdiffusive random process. Were cytoquakes a nonstationary cooperative process like an earthquake or avalanche, their time dependence, like the abrupt events, would have no reason to fit to the IEF model. The agreement of the IEF model across multiple cell types leads us to conclude that cytoquakes, at least in our data, are simply statistical mirages. Data for cytoquake and abrupt events in other cell types and conditions reinforce the above conclusions, see Fig. S6 [44].

The exponents for different cell types $\{a_{\rm IEF}\}$ for the gradual events agree well with the corresponding exponents $\{a_{\rm MSD}\}$ for the MSDs of the full trajectory datasets, Fig. 3(f) (see

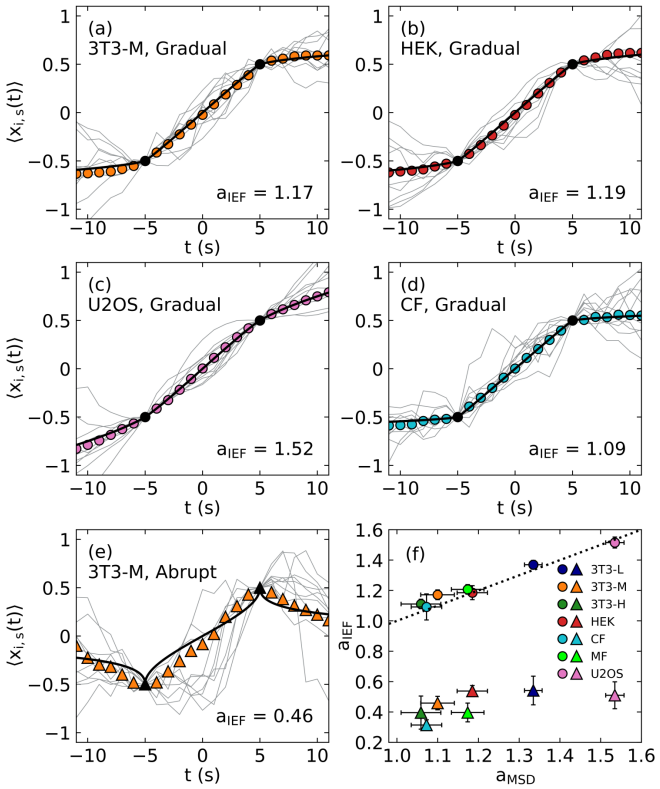

FIG. 3. Averaged scaled trajectories $\langle x_{i,s}(t)\rangle$ for large displacements are well described by the interpolation-extrapolation function (IEF). (a)–(d) $\langle x_{i,s}(t)\rangle$ for the 200 largest gradual displacements at $\tau = 10$ s, for four different cell types and conditions, as described in the text. Ten individual scaled trajectories $x_{i,s}(t)$ are superimposed in each case (gray). (e) $\langle x_{i,s}(t)\rangle$ for the 40 largest abrupt displacements for the 3T3 cells shown in (a). Solid lines in (a)–(e) are fits to the IEF, Eq. (2). (f) The exponents a_{IEF} from fitting the gradual IEFs (circles), and the corresponding MSD exponents a_{MSD} show close agreement. Additional datasets and fits to the IEF from Fig. S6 [44] are included in (f). The micropost stiffnesses were 3T3-L and U2OS: $k = 5.5\,\mathrm{nN/\mu m}$; 3T3-M and HEK: $k = 15.8\,\mathrm{nN/\mu m}$; 3T3-H, CF, and MF: $k = 22.3\,\mathrm{nN/\mu m}$. Dashed line: $a_{\mathrm{IEF}} = a_{\mathrm{MSD}}$. The a_{IEF} exponents for the abrupt displacements (triangles) differ widely from a_{MSD}. Error bars are standard errors, estimated from cell-to-cell variations [44]. The individual trajectories in (a)–(e) were chosen at random from the 50 largest [panels (a)–(d)] or 20 largest displacements [panel (e)].

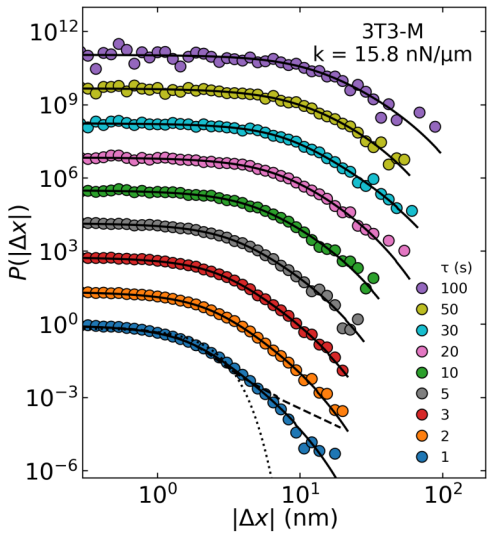

FIG. 4. The Van Hove fluctuation distributions for 3T3 cells are well described by an ETSD model (solid lines) over lag times τ from 1 to 100 s. The best-fit stable distribution (dashed line) shown at $\tau = 1$ s does not capture the behavior near the tail. The best-fit Gaussian is shown at $\tau = 1$ s for reference (dotted line). The distributions for $\tau > 1$ s are progressively offset by factors of $10^{1.5}$ for clarity. Micropost stiffness: $k = 15.8\,\mathrm{nm/\mu m}$ (medium stiffness).

Fig. S7 for MSD fits [44]). The agreement of these exponents confirms that the cytoquakes are driven by the same microscopic fluctuations and mechanics driving all cortical fluctuations. In contrast, the exponents for abrupt events differ significantly from $\{a_{\mathrm{MSD}}\}$, Fig. 3(f), confirming that they are due to a cellular process distinct from the other cortical fluctuations, e.g., micropost recoil after detachment from the cortex.

V. DISPLACEMENT DISTRIBUTIONS HAVE AN EXPONENTIALLY TRUNCATED STABLE DISTRIBUTION FORM

Our remaining task is to model the lag-time-dependent van Hove distribution that describes the cytoskeletal fluctuations. To do so, we must first screen out the above-described abrupt displacements. As the abrupt displacements were predominantly toward the posts' resting locations, we split the displacements into two sets: one with displacements moving toward the resting location, which we discarded, and the other for those moving away from it, which we retained (Fig. S5(e) [44]). Comparing these two sets of data suggests that the abrupt events (in the "toward" set) are responsible for about 20% of the total observed fluctuations on a power basis [44].

The cortical displacement distribution with abrupt events removed is shown in Fig. 4, plotted in log-log form for 3T3 cells and lag times from 1 to 100 s. Other cell types and conditions give similar results, shown in Fig. S8 [44]. We find that the cortical fluctuation distribution is well described by an exponentially truncated stable distribution (ETSD), given by

$$P(\Delta x) = A L_\alpha(\Delta x; \alpha, \gamma) e^{-\Delta x/\lambda}, \tag{3}$$

where $L_\alpha(\Delta x; \alpha, \gamma)$ is the symmetric Lévy α-stable distribution [47] with shape parameter α and scale parameter γ, A is a normalization constant, and λ is a truncation length. The ability to describe the entire distribution with a single function, as opposed to a sum of different functions, confirms our conclusion that we are observing the displacements of a single random process.

The ETSD parameters for our experiments, summarized in Fig. 5, vary significantly across cell types and post stiffness, with some displaying consistent trends versus lag time. This suggests that these measures are not "universal" and instead are sensitive to the arrangement of the cortical actin and myosin for different cell types and post stiffnesses. This is in contrast to the universal *rheology* of cells [4] and suggests

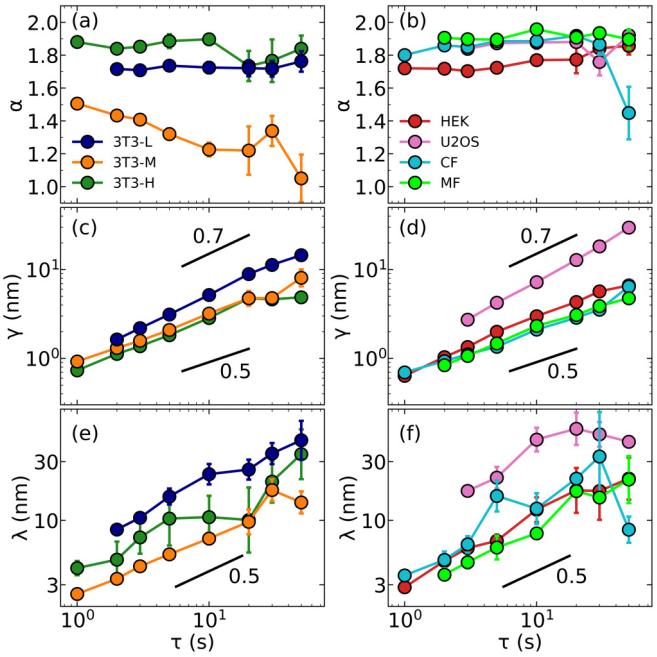

FIG. 5. The ETSD fit parameters vs lag time τ. (a) The shape parameter α varies with substrate stiffness. (b) The shape parameter α depends on the cell type. (c, d) The scale parameter γ follows a power law with exponent ≈0.7, corresponding to a superdiffusive MSD. The uncertainty in γ is smaller than the size of the markers. (e, f) The truncation parameter λ increases with increasing τ. Error bars are standard deviations of fits to samples drawn from the best-fit ETSDs to the experimental data.

that future actin and myosin perturbation experiments may elucidate the parameters' connections to cortical architecture.

VI. BIOPHYSICAL INTERPRETATION OF ETSD PARAMETERS

In this section we report the ETSD parameters and put them into biophysical context. The shape parameter $\alpha(\tau)$, Figs. 5(a) and 5(b), describes the exponent of the heavy tail, or equivalently, how non-Gaussian the displacements are versus lag time, τ ($\alpha = 2$ is Gaussian). Six out of seven conditions show modestly non-Gaussian behavior, $\alpha \approx 1.8$, essentially independent of lag time. Datasets collected on the high stiffness posts ($k = 22$ nN/μm) show the least non-Gaussian behavior, $\alpha \approx 1.9$. The 3T3 fibroblasts on medium stiffness posts (highlighted in previous figures) show very heavy-tailed displacements having a shape parameter that decreases with lag time.

Heavy-tailed fluctuations in conventional materials are caused by two distinct effects [33,34,48]. The first is geometrical due to the spatial decay of strain fields around force dipoles [32,48]. For the cortical geometry, a thin stiff sheet over a soft interior, this effect contributes negligible non-Gaussianity [32] and predicts $\alpha \approx 2$, inconsistent with our findings. The second effect is more direct: stable distributed displacements are the result of microscopic events (e.g., of forces or energy release) that themselves have a heavy-tailed distribution. In other words, non-Gaussian displacements are the result of non-Gaussian "noise" from microscopic processes. In this case the tail exponent of the noise amplitude distribution is connected to the stability parameter α of the mesoscopic displacement [33,34] via a generalized central limit theorem [49]. Biophysically, our findings suggest that the ETSD distribution of cortical displacements is the result of a heavy-tailed distribution of the random microscopic forces or energy release events driving the fluctuations of the cortex.

The scale parameter $\gamma(\tau)$ of the displacement distributions, Figs. 5(c) and 5(d), is akin to the width or "knee" of the distribution and grows with τ, as is evident in Fig. 4. The displacement scales are fairly similar across cell types at a given substrate stiffness, with intuitively larger displacement scales being observed on softer posts. The scale parameters increase as power laws of lag time, with exponents in the range 0.5–0.7. For a truncated distribution, the scale parameter and standard deviation are correlated, so the mean-squared displacement should scale $\sim\gamma^2$. Thus our findings appear consistent with the well-known [4,8,29] superdiffusive nature of cortical fluctuations, having nonuniversal exponents in the range 1.0–1.4 [2,8,11,16,29]. A classic model of stationary superdiffusive processes is fractional Brownian motion (FBM) [46], which combines Gaussian noise with a power-law memory kernel. The FBM model has been extended to include noise having a stable distribution form, termed linear fractional stable motion (LFSM) [33,34], a process that displays both superdiffusion and displacements that follow a stable distribution at all lag times. Notably, an LFSM process creates "power-law" distributed displacements without an earthquakelike mechanism. Biophysically, a LFSM process would correspond to the cortex being driven by uncorrelated heavy-tailed noise, with a power-law memory kernel provided by the cortex's power-law creep compliance and/or temporal correlations in the noise.

The truncation parameter $\lambda(\tau)$, Figs. 5(e) and 5(f), describes the effective maximum size of a displacement that occurs in time τ; larger events are exponentially rare. If the displacements are driven by non-Gaussian noise from microscopic events having a heavy-tailed distribution, then the observed truncation simply suggests that these events have a well-defined maximum size. Such truncation is ubiquitous in physical systems but not present in existing LFSM models. We find experimentally that the truncation length increases with τ, as roughly $\sim\tau^{1/2}$. We conjecture that such scaling corresponds to a diffusionlike process: $\lambda(\tau) = \lambda_0\sqrt{k_{\max}\tau}$, where λ_0 is the displacement due to a maximum-sized single microscopic event, and $k_{\max}$ is the rate at which such events occur. In this picture, at longer lag times many maximal microscopic events have contributed to a maximal micropost displacement, whose uncorrelated effects add together as in a random walk.

The truncation length scale $\lambda(\tau)$ we measure describes the displacement of a mesoscopic micropost and not any structure in the cortex, such as myosin stepping. As such it is interesting to convert it to the work done on the micropost by the cortex via the formula for the elastic energy in a spring $\Delta U_{\text{post}} = \frac{1}{2}k\Delta x^2$. The maximum displacement $\Delta x = \lambda(\tau = 1\text{ s}) = 3$ nm and $k = 15.8$ nN/μm yields an energy of $\Delta U_{\text{post}} = 7 \times 10^{-20}$ J. This energy represents a lower bound for the largest energy release events driving cortical

fluctuations, assuming that a single such event is responsible for a λ-sized micropost displacement (see SM for details [44].) If our displacements at $\tau = 1$ s actually correspond to multiple such maximal events, the microscopic events' energy could be even lower. It is useful to compare this energy bound to the characteristic elastic energy in cortical elements, such as highly stretched actin filaments [50–52]. Following a recent computational model for the cortex [53] which suggests that individual actin filaments are stretched to very high tensions up to 400 pN (about 2/3 of their breaking tension [54]), we can estimate the maximal elastic energy stored in a single cortical actin filament: $\Delta U_{\text{actin}} = 20 \times 10^{-20}$ J (see SM for details [44]). Notably, the fact that the estimated lower bound of the (λ-scale) energy release event ΔU_{post} is only about a third of the value of ΔU_{actin} implies that even the largest cortical fluctuations we observe could be readily driven by single microscopic processes in the cortex.

VII. DISCUSSION

The first paper on cytoquakes [18] as well as our subsequent papers [8,29] hypothesize that they are due to the collective or cooperative reconfiguration of many microscopic degrees of freedom, with one microscopic event triggering many more in the manner of an avalanche or earthquake. This hypothesis is motivated by the power-law-distributed displacement distributions that we observe in detail here. Moreover, the largest reported cytoquakes, often up to 30 nm in 10 s, correspond to large work done on the micropost, $\Delta U_{\text{quake}} = 7 \times 10^{-18}$ J, far larger than the typical energy in a tensed cortical actin filament (see SM [44]). Such large cytoquake energies are consistent with the hypothesis of many cytoskeleton elements cooperatively rupturing or reconfiguring.

In contrast, however, a major finding of this study is that cytoquakes closely resemble chance large excursions of a stationary random process driven by non-Gaussian noise (as in Fig. 3). The time-dependent shape and power-law distribution of the largest cytoquakes can thus be explained as the chance result of many statistically uncorrelated microscopic events having a heavy-tailed distribution of energy, without any earthquakelike cooperativity. Moreover, analysis of the truncation parameter λ suggests that the largest single microscopic energy release events driving cortical motion are comparable to the energy in single tensed actin filaments. Rather than being a mechanical network near some mechanical critical point subject to "earthquakes," the cytoskeleton may simply be a mechanical network with little or no cooperativity driven by active stresses due to structural changes of single cortical elements.

Next, we consider possible physical origins of the random process driving both the observed cortical fluctuations having an ETSD form and the occasional cytoquakes. It is well accepted that the mechanical energy in the cortex comes from myosin II contraction, and molecular stepping has been seen in cortex-adhered microposts associated with large myosin contractile units [40]. FRAP experiments [35] show rapid cortical turnover, with the average tensed actin filament lifetime being only 30 s. The removal of filaments is primarily due to cofilin severing followed by depolymerization. This severing process, or similarly, the unbinding of tensed actin filaments from myosin minifilaments or crosslinking molecules, would abruptly release the stored elastic energy in the tensed actin filament and cause the surrounding network to recoil. This recoil energy would have the correct magnitude to account for our observed fluctuations, and these events would likely have a broad distribution of energies related to the expected broad distribution of filament tensions [53]. A suitably broad distribution could then lead, potentially, to the heavy-tailed noise implied by our ETSD fluctuations. Alternatively, the distribution of microscopic elastic energies may not be heavy tailed, and the heavy-tailed active noise may be due to cooperativity among energy release events on the microscale, as seen in recent simulations [31].

Our fluctuation measurements suggest that the actomyosin cortex is driven by highly non-Gaussian noise due to microscopic processes releasing energies less than the typical elastic energy in single cortical actin filaments. While these microscopic processes may display some cooperativity, such cooperativity is not required to explain the cytoquake phenomenon. The observed ETSD distribution of the fluctuations is both a clue to direct the development of new physical models and a challenge for existing ones to reproduce, for example, through a broad distribution of elastic energies in actin filaments or other mechanical elements. The ETSD distribution closely resembles that seen in soft glassy materials [28], adding to the curious similarity between the cytoskeleton and SGMs [1], but this could be explained if both are simply viscoelastic solids driven by highly non-Gaussian active noise. Unlike cell rheology curves, which are parameterized by a single, nearly universal exponent [4], the measured lag-time-dependent ETSD parameters appear sensitive to cell-type-specific details of actomyosin assembly. Further experiments to link these distribution parameters to actomyosin structure and biochemistry should be useful in enabling the refinement of future models.

ACKNOWLEDGMENTS

We are grateful to B. Camley for helpful discussions, C. S. Chen for donation of mPAD masters, and T. Schroer for donation of U2OS cells. This work was supported by NSF Grants No. PHY-1915193 and No. PHY-1915174, and NIH Grant No. R01 HL127087.

[1] B. Fabry, G. N. Maksym, J. P. Butler, M. Glogauer, D. Navajas, and J. J. Fredberg, Scaling the microrheology of living cells, Phys. Rev. Lett. **87**, 148102 (2001).

[2] B. D. Hoffman, G. Massiera, K. M. Van Citters, and J. C. Crocker, The consensus mechanics of cultured mammalian cells, Proc. Natl. Acad. Sci. USA **103**, 10259 (2006).

[3] J. Solon, I. Levental, K. Sengupta, P. C. Georges, and P. A. Janmey, Fibroblast adaptation and stiffness matching to soft elastic substrates, Biophys. J. **93**, 4453 (2007).

[4] B. D. Hoffman and J. C. Crocker, Cell mechanics: Dissecting the physical responses of cells to force, Annu. Rev. Biomed. Eng. **11**, 259 (2009).

[5] S.-Y. Tee, J. Fu, C. S. Chen, and P. A. Janmey, Cell shape and substrate rigidity both regulate cell stiffness, Biophys. J. **100**, L25 (2011).

[6] R. Vargas-Pinto, H. Gong, A. Vahabikashi, and M. Johnson, The effect of the endothelial cell cortex on atomic force microscopy measurements, Biophys. J. **105**, 300 (2013).

[7] A. Rigato, A. Miyagi, S. Scheuring, and F. Rico, High-frequency microrheology reveals cytoskeleton dynamics in living cells, Nat. Phys. **13**, 771 (2017).

[8] Y. Shi, C. L. Porter, J. C. Crocker, and D. H. Reich, Dissecting fat-tailed fluctuations in the cytoskeleton with active micropost arrays, Proc. Natl. Acad. Sci. USA **116**, 13839 (2019).

[9] M. L. Gardel, J. H. Shin, F. C. MacKintosh, L. Mahadevan, P. Matsudaira, and D. A. Weitz, Elastic behavior of cross-linked and bundled actin networks, Science **304**, 1301 (2004).

[10] D. Mizuno, C. Tardin, C. F. Schmidt, and F. C. MacKintosh, Nonequilibrium mechanics of active cytoskeletal networks, Science **315**, 370 (2007).

[11] X. Trepat, L. Deng, S. S. An, D. Navajas, D. J. Tschumperlin, W. T. Gerthoffer, J. P. Butler, and J. J. Fredberg, Universal physical responses to stretch in the living cell, Nature (London) **447**, 592 (2007).

[12] M. Balland, N. Desprat, D. Icard, S. Féréol, A. Asnacios, J. Browaeys, S. Hénon, and F. Gallet, Power laws in microrheology experiments on living cells: Comparative analysis and modeling, Phys. Rev. E **74**, 021911 (2006).

[13] K. K. Mandadapu, S. Govindjee, and M. R. Mofrad, On the cytoskeleton and soft glassy rheology, J. Biomech. **41**, 1467 (2008).

[14] A. Caspi, R. Granek, and M. Elbaum, Enhanced diffusion in active intracellular transport, Phys. Rev. Lett. **85**, 5655 (2000).

[15] A. W. C. Lau, B. D. Hoffmann, A. Davies, J. C. Crocker, and T. C. Lubensky, Microrheology, stress fluctuations, and active behavior of living cells, Phys. Rev. Lett. **91**, 198101 (2003).

[16] M. Guo, A. J. Ehrlicher, M. H. Jensen, M. Renz, J. R. Moore, R. D. Goldman, J. Lippincott-Schwartz, F. C. Mackintosh, and D. A. Weitz, Probing the stochastic, motor-driven properties of the cytoplasm using force spectrum microscopy, Cell **158**, 822 (2014).

[17] P. Bursac, G. Lenormand, B. Fabry, M. Oliver, D. A. Weitz, V. Viasnoff, J. P. Butler, and J. J. Fredberg, Cytoskeletal remodelling and slow dynamics in the living cell, Nat. Mater. **4**, 557 (2005).

[18] A. M. Alencar, M. S. A. Ferraz, C. Y. Park, E. Millet, X. Trepat, J. J. Fredberg, and J. P. Butler, Non-equilibrium cytoquake dynamics in cytoskeletal remodeling and stabilization, Soft Matter **12**, 8506 (2016).

[19] C. P. Broedersz, M. Depken, N. Y. Yao, M. R. Pollak, D. A. Weitz, and F. C. MacKintosh, Cross-link-governed dynamics of biopolymer networks, Phys. Rev. Lett. **105**, 238101 (2010).

[20] Y. Mulla, F. C. MacKintosh, and G. H. Koenderink, Origin of slow stress relaxation in the cytoskeleton, Phys. Rev. Lett. **122**, 218102 (2019).

[21] S. Chen, C. P. Broedersz, T. Markovich, and F. C. MacKintosh, Nonlinear stress relaxation of transiently crosslinked biopolymer networks, Phys. Rev. E **104**, 034418 (2021).

[22] P. Hébraud and F. Lequeux, Mode-coupling theory for the pasty rheology of soft glassy materials, Phys. Rev. Lett. **81**, 2934 (1998).

[23] P. Sollich, F. Lequeux, P. Hébraud, and M. E. Cates, Rheology of soft glassy materials, Phys. Rev. Lett. **78**, 2020 (1997).

[24] P. Sollich, Rheological constitutive equation for a model of soft glassy materials, Phys. Rev. E **58**, 738 (1998).

[25] H. J. Hwang, R. A. Riggleman, and J. C. Crocker, Understanding soft glassy materials using an energy landscape approach, Nat. Mater. **15**, 1031 (2016).

[26] F. Giavazzi, V. Trappe, and R. Cerbino, Multiple dynamic regimes in a coarsening foam, J. Phys.: Condens. Matter **33**, 024002 (2021).

[27] F. A. Lavergne, P. Sollich, and V. Trappe, Delayed elastic contributions to the viscoelastic response of foams, J. Chem. Phys. **156**, 154901 (2022).

[28] C. Rodríguez-Cruz, M. Molaei, A. Thirumalaiswamy, K. Feitosa, V. N. Manoharan, S. Sivarajan, D. H. Reich, R. A. Riggleman, and J. C. Crocker, Experimental observations of fractal landscape dynamics in a dense emulsion, Soft Matter **19**, 6805 (2023).

[29] Y. Shi, S. Sivarajan, K. M. Xiang, G. M. Kostecki, L. Tung, J. C. Crocker, and D. H. Reich, Pervasive cytoquakes in the actomyosin cortex across cell types and substrate stiffness, Integr. Biol. **13**, 246 (2021).

[30] J. Liman, C. Bueno, Y. Eliaz, N. P. Schafer, M. N. Waxham, P. G. Wolynes, H. Levine, and M. S. Cheung, The role of the Arp2/3 complex in shaping the dynamics and structures of branched actomyosin networks, Proc. Natl. Acad. Sci. USA **117**, 10825 (2020).

[31] C. Floyd, H. Levine, C. Jarzynski, and G. A. Papoian, Understanding cytoskeletal avalanches using mechanical stability analysis, Proc. Natl. Acad. Sci. USA **118**, e2110239118 (2021).

[32] D. W. Swartz and B. A. Camley, Active gels, heavy tails, and the cytoskeleton, Soft Matter **17**, 9876 (2021).

[33] S. Stoev and M. S. Taqqu, Simulation methods for linear fractional stable motion and FARIMA using the fast Fourier transform, Fractals **12**, 95 (2004).

[34] K. Burnecki and A. Weron, Fractional Lévy stable motion can model subdiffusive dynamics, Phys. Rev. E **82**, 021130 (2010).

[35] M. Fritzsche, A. Lewalle, T. Duke, K. Kruse, and G. Charras, Analysis of turnover dynamics of the submembranous actin cortex, Mol. Biol. Cell **24**, 757 (2013).

[36] J. L. Tan, J. Tien, D. M. Pirone, D. S. Gray, K. Bhadriraju, and C. S. Chen, Cells lying on a bed of microneedles: An approach to isolate mechanical force, Proc. Natl. Acad. Sci. USA **100**, 1484 (2003).

[37] O. du Roure, A. Saez, A. Buguin, R. H. Austin, P. Chavrier, P. Siberzan, and B. Ladoux, Force mapping in epithelial cell migration, Proc. Natl. Acad. Sci. **102**, 2390 (2005).

[38] N. J. Sniadecki, A. Anguelouch, M. T. Yang, C. M. Lamb, Z. Liu, S. B. Kirschner, Y. Liu, D. H. Reich, and C. S. Chen, Magnetic microposts as an approach to apply forces to living cells, Proc. Natl. Acad. Sci. USA **104**, 14553 (2007).

[39] Y. Geng and Z. Wang, Review of cellular mechanotransduction on micropost substrates, Med. Biol. Eng. Comput. **54**, 249 (2016).

[40] H. Wolfenson, G. Meacci, S. Liu, M. R. Stachowiak, T. Iskratsch, S. Ghassemi, P. Roca-Cusachs, B. O'Shaughnessy, J. Hone, and M. P. Sheetz, Tropomyosin controls sarcomere-like contractions for rigidity sensing and suppressing growth on soft matrices, Nat. Cell Biol. **18**, 33 (2016).

[41] J. Fu, Y.-K. Wang, M. T. Yang, R. A. Desai, X. Yu, Z. Liu, and C. S. Chen, Mechanical regulation of cell function with geometrically modulated elastomeric substrates, Nat. Methods **7**, 733 (2010).

[42] Y. Shi, S. Sivarajan, J. C. Crocker, and D. H. Reich, Measuring cytoskeletal mechanical fluctuations and rheology with active micropost arrays, Curr. Protocol. **2**, e433 (2022).

[43] S. Weng and J. Fu, Synergistic regulation of cell function by matrix rigidity and adhesive pattern, Biomaterials **32**, 9584 (2011).

[44] See Supplemental Material at http://link.aps.org/supplemental/10.1103/PhysRevResearch.6.043265 for expanded methods and supplementary figures.

[45] J. C. Crocker and D. G. Grier, Methods of digital video microscopy for colloidal studies, J. Colloid Interface Sci. **179**, 298 (1996).

[46] B. B. Mandelbrot and J. W. Van Ness, Fractional Brownian motions, fractional noises and applications, SIAM Rev. **10**, 422 (1968).

[47] V. Zaburdaev, S. Denisov, and J. Klafter, Lévy walks, Rev. Mod. Phys. **87**, 483 (2015).

[48] L. Cipelletti, L. Ramos, S. Manley, E. Pitard, D. A. Weitz, E. E. Pashkovski, and M. Johansson, Universal non-diffusive slow dynamics in aging soft matter, Faraday Discuss. **123**, 237 (2003).

[49] V. V. Uchaikin and V. M. Zolotarev, *Chance and Stability: Stable Distributions and Their Applications* (Walter de Gruyter, 2011).

[50] H. Kojima, A. Ishijima, and T. Yanagida, Direct measurement of stiffness of single actin filaments with and without tropomyosin by in vitro nanomanipulation, Proc. Natl. Acad. Sci. USA **91**, 12962 (1994).

[51] X. Liu and G. H. Pollack, Mechanics of F-Actin characterized with microfabricated cantilevers, Biophys. J. **83**, 2705 (2002).

[52] S. Matsushita, T. Adachi, Y. Inoue, M. Hojo, and M. Sokabe, Evaluation of extensional and torsional stiffness of single actin filaments by molecular dynamics analysis, J. Biomech. **43**, 3162 (2010).

[53] M. A. Galvani Cunha, J. C. Crocker, and A. J. Liu, Building rigid networks with prestress and selective pruning, Phys. Rev. Res. **6**, L042020 (2024).

[54] Y. Tsuda, H. Yasutake, A. Ishijima, and T. Yanagida, Torsional rigidity of single actin filaments and actin–actin bond breaking force under torsion measured directly by *in vitro* micromanipulation, Proc. Natl. Acad. Sci. **93**, 12937 (1996).